

Two-dimensional tetragonal ZnB: A nodalline semimetal with good transport properties

Yong-Chun Zhao(赵永春), Ming-Xin Zhu(朱铭鑫), Sheng-Shi Li(李胜世), and Ping Li(李萍)
Citation: Chin. Phys. B, 2023, 32 (**6**): 067301. DOI: 10.1088/1674-1056/ac8f33
Journal homepage: http://cpb.iphy.ac.cn; http://iopscience.iop.org/cpb

What follows is a list of articles you may be interested in

Room temperature quantum anomalous Hall insulator in honeycomb lattice, $RuCS_3$, with large magnetic anisotropy energy

Yong-Chun Zhao(赵永春), Ming-Xin Zhu(朱铭鑫), Sheng-Shi Li(李胜世), and Ping Li(李萍)
Chin. Phys. B, 2023, 32 (**5**): 057301. DOI: 10.1088/1674-1056/aca396

Chiral symmetry protected topological nodal superconducting phase and Majorana Fermi arc

Mei-Ling Lu(卢美玲), Yao Wang(王瑶), He-Zhi Zhang(张鹤之), Hao-Lin Chen(陈昊林), Tian-Yuan Cui(崔天元), and Xi Luo(罗熙)
Chin. Phys. B, 2023, 32 (**2**): 027301. DOI: 10.1088/1674-1056/ac7208

Effects of preparation parameters on growth and properties of β-Ga_2O_3 film

Zi-Hao Chen(陈子豪), Yong-Sheng Wang(王永胜), Ning Zhang(张宁), Bin Zhou(周兵), Jie Gao(高洁), Yan-Xia Wu(吴艳霞), Yong Ma(马永), Hong-Jun Hei(黑鸿君), Yan-Yan Shen(申艳艳), Zhi-Yong He(贺志勇), and Sheng-Wang Yu(于盛旺)
Chin. Phys. B, 2023, 32 (**1**): 017301. DOI: 10.1088/1674-1056/ac728c

Hexagonal boron phosphide and boron arsenide van der Waals heterostructure as high-efficiency solar cell

Yi Li(李依), Dong Wei(魏东), Gaofu Guo(郭高甫), Gao Zhao(赵高), Yanan Tang(唐亚楠), and Xianqi Dai(戴宪起)
Chin. Phys. B, 2022, 31 (**9**): 097301. DOI: 10.1088/1674-1056/ac6b2a

Precisely controlling the twist angle of epitaxial MoS_2/graphene heterostructure by AFM tip manipulation

Jiahao Yuan(袁嘉浩), Mengzhou Liao(廖梦舟), Zhiheng Huang(黄智恒), Jinpeng Tian(田金朋), Yanbang Chu(褚衍邦), Luojun Du(杜罗军), Wei Yang(杨威), Dongxia Shi(时东霞), Rong Yang(杨蓉), and Guangyu Zhang(张广宇)
Chin. Phys. B, 2022, 31 (**8**): 087302. DOI: 10.1088/1674-1056/ac720e

---

Two-dimensional tetragonal ZnB: A nodalline semimetal with good transport properties

Yong-Chun Zhao(赵永春)[1], Ming-Xin Zhu(朱铭鑫)[1], Sheng-Shi Li(李胜世)[2], and Ping Li(李萍)[1,†]

[1] *School of Physics and Technology, University of Jinan, Jinan* 250022, *China*
[2] *Institute of Spintronics, University of Jinan, Jinan* 250022, *China*

(Received 19 May 2022; revised manuscript received 30 August 2022; accepted manuscript online 5 September 2022)

Nodal-line semimetals have become a research hot-spot due to their novel properties and great potential application in spin electronics. It is more challenging to find 2D nodal-line semimetals that can resist the spin–orbit coupling (SOC) effect. Here, we predict that 2D tetragonal ZnB is a nodal-line semimetal with great transport properties. There are two crossing bands centered on the *S* point at the Fermi surface without SOC, which are mainly composed of the p_{xy} orbitals of Zn and B atoms and the p_z orbitals of the B atom. Therefore, the system presents a nodal line centered on the *S* point in its Brillouin zone (BZ). And the nodal line is protected by the horizontal mirror symmetry M_z. We further examine the robustness of a nodal line under biaxial strain by applying up to -4% in-plane compressive strain and 5% tensile strain on the ZnB monolayer, respectively. The transmission along the *a* direction is significantly stronger than that along the *b* direction in the conductive channel. The current in the *a* direction is as high as 26.63 μA at 0.8 V, and that in the *b* direction reaches 8.68 μA at 0.8 V. It is interesting that the transport characteristics of ZnB show the negative differential resistance (NDR) effect after 0.8 V along the *a* (*b*) direction. The results provide an ideal platform for research of fundamental physics of 2D nodal-line fermions and nanoscale spintronics, as well as the design of new quantum devices.

Keywords: nodal-line semimetals, negative differential resistance (NDR) effect, horizontal mirror symmetry

PACS: 73.20.At, 62.20.D–, 72.10.–d **DOI:** 10.1088/1674-1056/ac8f33

1. Introduction

The discovery of graphene[1–5] opens the door to "Dirac physics". The conduction and valence bands of two-dimensional (2D) Dirac materials cross linearly at Fermi points in the Brillouin zone (BZ). Dirac fermions[6] cause the electron transport of the 2D Dirac materials to exhibit novel properties, such as high carrier mobility,[7] ballistic charge transport[8] and quantum Hall effects.[9,10] Dirac materials have been extended to many other 2D lattices in addition to graphene, for example, silicene,[11] phagraphene,[12] Bi/Sb (111) films,[13] square lattice tellurium,[14] square SbI[15] and MoS_2.[16] They have broad application prospects in the design of nanoelectronic devices. The band crossings can not only be expressed as Dirac points, but also as nodal lines. Nodal-line semimetals[17] have one-dimensional line bands formed by crossing several bands near the Fermi surface. The nodal lines were first discovered in 3D materials, such as $PtSn_4$,[18] ZrSiS,[19] Mackay–Terrones crystals[20] and anti-perovskite Cu_3PdN.[21] Recently, several 2D nodal-line materials,[22–26] such as *M*X (*M* = Pd, Pt; *X* = S, Se, Te)[22] and the bipartite square lattice,[23] have been predicted theoretically. In addition, the existence of nodal lines with two concentric lines centered on the Γ point in monolayer Cu_2Si and CuSe has been confirmed experimentally.[27,28] The existence of a nodal line requires certain symmetry protection, in which the horizontal mirror symmetry M_z is the most prevalent. There are many horizontal mirror-symmetric structures. Recent work has shown that AuSe[29] is a two-dimensional material that can be successfully prepared experimentally. We expanded our attention to *XY* (*X* = Zn, Ag, Au, Cu; *Y* = B, C, N, O) monolayers, which share a similar structure to AuSe. Figure S2 shows the corresponding band structures. Additionally, the results of band structure calculations reveal that ZnB exhibits nodal-line characteristics in its Brillouin zone (BZ). In this work, the structure of ZnB is derived from AuSe and, on this basis, Zn and B atoms replace Au and Se atoms. After structural relaxation, two dimensional ZnB monolayers were obtained.

The ZnB material studied in this paper is Dirac material. The presence of Dirac cones usually results in materials with excellent electron transport properties. An interesting phenomenon in electron transport is the negative differential resistance (NDR) effect,[30] which refers to the phenomenon whereby the voltage (or current) decreases as the current (or voltage) increases. The effect of this phenomenon on the circuit is equivalent to a negative resistance; therefore, it is called the "NDR effect". The NDR effect was first observed by Esaki in 1958 when he studied p-n junction tunneling diodes.[31] Esaki and Tsu jointly proposed that NDR can also be achieved in the current passing through quantum wells in 1973.[32] Only a few years later, NDR was observed in a GaAs/$Ga_{1-x}Al_xAs$ superlattice. In the mid-1980s, quantum well devices were manufactured as standard in experimental growth deposition

†Corresponding author. E-mail: ss_lip@ujn.edu.cn
© 2023 Chinese Physical Society and IOP Publishing Ltd

systems for heterostructures based on the NDR effect.[33] Recently, the NDR effect was predicted in the halfmetallic MnNF monolayer with a nodal loop. The NDR effect can be used to design high-frequency oscillators and alternating current amplifiers to generate oscillations and amplify electrical signals. By calculating the transport properties of ZnB, it is found that ZnB also has an NDR effect. This NDR effect has potential value in practice. In this work, we structure a 2D tetragonal ZnB material, and we confirmed that 2D tetragonal ZnB is a nodal-line semimetal with good transport properties and NDR effects based on first-principles calculations. We also confirmed the mechanical and dynamics stability of the system by calculating the cohesive energy, linear elastic constant and phonon spectrum. The system exhibits nodal-line characteristics in its Brillouin zone (BZ). It is worth noting that the nodal line is protected by the mirror inversion symmetry and p_{xy}/p_z band inversion. We found that only the tiny band gaps of 8 meV and 9 meV are opened at Dirac cones when SOC is turned on. Therefore, the nodal line is robust to SOC. We also confirmed its robustness under biaxial strain. Our conclusions provide new ideas for the study of nanoscale spintronics and the design of new quantum devices.

2. Computational methods

First-principles calculations based on density functional theory (DFT) were performed using the Vienna *ab-initio* simulation package (VASP).[34,35] We processed the exchange–correlation function using generalized gradient approximation (GGA)[39,40] in the form of Perdew—Burke–Ernzerhof (PBE).[36–38] When constructing the structure, a vacuum layer greater than 20 Å is added in the z direction to eliminate interactions between adjacent layers. In the calculation process, the cutoff energy of the plane wave is set to 500 eV, and the energy convergence standard is 1×10^{-6} eV. When optimizing the structure, Monkhorst–Pack meshes of $9\times9\times1$ k-points are used for sampling in the two-dimensional Brillouin zone (BZ), and the interaction force between the atoms is less than 0.01 eV/Å. The phonon calculations are based on DFT perturbation theory using the PHONOPY code[41] in VASP. The HSE06 hybrid functional is used to confirm the reliability of our PBE results. All calculations were performed using the GGA$+U$ ($U=3.0$ eV) method,[42] and the effective parameter $U_{\rm eff}$ was set to explain the Coulomb interaction between the 3d electrons. The transport properties were calculated using the nonequilibrium Green function (NEGF) method,[43–46] as implemented in the OpenMX code.

3. Results and discussion

Figure 1(a) shows top and side views of the ZnB structure, respectively. The ZnB lattice forms 2D networks of a rectangular lattice in the xy plane. The space group is *Pmmm* with the point group D_{2H-1}. Each unit cell contains two Zn atoms and two B atoms. After structural relaxation, the crystal constants along the x and y directions are 3.86 Å and 5.53 Å, respectively. All the bond lengths labeled in Fig. 1(a) are $d_1=1.547$ Å (between two B atoms), $d_2=1.990$ Å (between B and Zn atoms) and $d_3=2.081$ Å (between B and Zn atoms). To determine the stability of ZnB, we first calculate its cohesive energy, and the formula is expressed as

$$E_{\rm coh}=\left(E_{\rm ZnB}-2E_{\rm Zn}-2E_{\rm B}\right)/4, \tag{1}$$

where $E_{\rm ZnB}$ is the total energy of ZnB. Here, $E_{\rm Zn}$ and $E_{\rm B}$ are the energies of free Zn and B atoms, respectively. The calculated $E_{\rm coh}$ is -3.25 eV/atom. The cohesive energy of ZnB is slightly lower than that of single-layer metal halide $MnCl_2$ (-3.23 eV/atom) exfoliated from its bulk,[46] which indicates that ZnB is stable and easy to prepare. We further perform the phonon spectrum calculations shown in Fig. 1(b); no appreciable imaginary phonon modes are observed, indicating that this structure is dynamically stable.

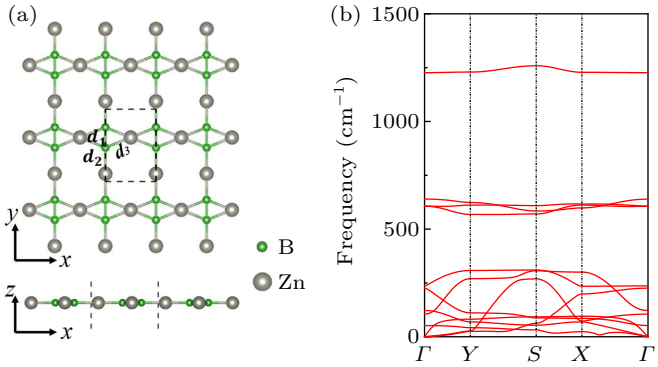


Fig. 1. (a) Top and side views of the ZnB structure. (b) The calculated phonon spectra of ZnB.

We studied the mechanical properties of ZnB by calculating the linear elastic constant. From calculation, the four independent elastic constants of ZnB are $C_{11}=300.82$ N·m^{-1}, $C_{22}=473.37$ N·m^{-1}, $C_{12}=12.99$ N·m^{-1} and $C_{66}=0.17$ N·m^{-1}, respectively. Their relationship is in accordance with Born criteria:[47,48] $C_{11}C_{22}-C_{12}^2>0$ and $C_{66}>0$, which satisfies the mechanical equilibrium conditions.[49] Therefore, ZnB has mechanical stability. The Young's modulus $Y(\theta)$ and Possion's ratio $\upsilon(\theta)$ of ZnB with the arbitrary in-plane θ is calculated using the following formula:

$$Y(\theta)=\frac{C_{11}C_{22}-C_{12}^2}{C_{11}\sin^4\theta+A\sin^2\theta\cos^2\theta+C_{22}\cos^4\theta}, \tag{2}$$

$$\nu(\theta)=\frac{C_{12}\sin^4\theta-B\sin^2\theta\cos^2\theta+C_{22}\cos^4\theta}{C_{11}\sin^4\theta+A\sin^2\theta\cos^2\theta+C_{22}\cos^4\theta}. \tag{3}$$

Here, $A = (C_{11}C_{22} - C_{12}^2)/C_{66} - 2C_{12}$ and $B = C_{11} + C_{22} - (C_{11}C_{22} - C_{12}^2)/C_{66}$. As seen in Fig. 2(a), Young's modulus in the x and y directions is 75.12 N·m^{-1} and 118.20 N·m^{-1}, respectively, indicating that ZnB has anisotropic mechanical behavior. Figure 2(b) shows that the Poisson's ratios of ZnB are between 0 and 0.5, which are similar to most previously reported 2D materials. These moderate values indicate that the structure can be regulated under external stress.

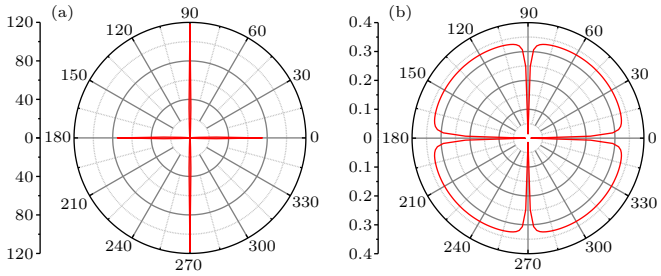


Fig. 2. Polar diagrams for (a) Young's modulus $Y(\theta)$ and (b) Poisson's ratio $\upsilon(\theta)$ of 2D ZnB.

We use the DFT + U (U = 3.0 eV) method to calculate band structures of ZnB because the DFT + PBE method cannot accurately describe the physical properties of transition metal Zn with Coulomb interactions between 3d electrons. Figure 4(a) shows the band structures of ZnB without SOC. Two linear band crossings are observed on the Fermi level, and they are labeled as α and β, respectively. The energy band intersections R_1 and R_2 are along the S–Y and S–Γ lines, respectively. Due to the existence of Dirac cones, we expect ZnB to have excellent electronic transport properties. Therefore, we calculate the Fermi velocity v_{F} for R_1 and R_2 points according to

$$v_{\mathrm{F}} = \frac{1}{\hbar}\frac{\partial E}{\partial k}. \tag{4}$$

Here, the v_{F} after unit conversion is expressed as

$$v_{\mathrm{F}} = \frac{\mathrm{d}E}{\mathrm{d}k} = \frac{\Delta E \times 1.6 \times 10^{-19} \times a \times 10^{-10}}{\frac{\Delta k}{k_{\mathrm{t}}} \times \frac{4\pi}{3} \times 1.0545 \times 10^{-34}}, \tag{5}$$

where k_{t} is the total number of points from S–Y (S–Γ), Δk is the number of K points on a certain energy band between S–Y (S–Γ), ΔE is the energy band, and a is the lattice constant of the structure. We find that the radial velocities of the Dirac point are 4.97×10^5 m/s and 4.70×10^5 m/s, respectively. They are even comparable to graphene (9.42×10^5 m/s).[50] At the same time, the linear dispersion of energy bands indicates that effective electron mass at the Dirac cone is almost zero, and that of $3 \times 10^{-5} m_0$ (m_0 is the static effective mass of electrons) of ZnB also confirms this conclusion. In addition, we calculated energy bands without SOC using the highly accurate and reliable HSE06 hybrid function (Fig. 4(c)). The calculated results agree with those of PBE, and the bands do not open the gap using the HSE method. Figure 4(b) depicts the component analysis of energy bands by the DFT + U method. We find that the α band is mainly contributed by p_{xy} orbitals of Zn and B atoms, and the β band is mainly contributed by the p_z orbital of the B atom. The inverted gap formed by the band inversion between the conduction band and valence band is 1.51 eV. Under the actions of the spatial inversion symmetric operator, the parity of wave functions of two bands, p_{xy} and p_z, is opposite, which prevents the interaction between p_{xy} and p_z states. Therefore, bands produce closed gaps around the S point, and no gaps are generated, even if they are far away from the high-symmetry line. It is worth noting that the band inversion causes the conduction band and the valence band to continuously cross, and the cross forms a continuous loop in the momentum space, which forms the typical nodal line. The DOS (Fig. S1) indicates that the valence band near the Fermi level is mainly contributed by the p-orbitals of B and the p_{xy}-orbitals of Zn atoms. The conduction band near the Fermi level is mainly contributed by the p_z-orbitals of B and the p_{xy}-orbitals of Zn atoms. In addition, the existence of a nodal line requires certain symmetry protection. For the ZnB monolayer, the space group *Pmmm* contains eight symmetry operators, i.e., one identity operator (E), one inversion operator (I), three mirror planes (M_x, M_y and M_z) and three rotation axis (C_{2x}, C_{2y} and C_{2z}). The structure has horizontal mirror symmetry M_z parallel to the 2D lattice due to the coplanarity of all Zn and B atoms (Fig. 1(a)). To obtain insight into the protection mechanism, the real-space Kohn–Sham wave functions near the nodal lines are plotted in Fig. 3. As shown in Fig. 3, the two bands forming the nodal line have opposite M_Z eigenvalues: the hole-like band α has the M_Z eigenvalue +i, whereas the electron-like band β has the eigenvalue −i. Therefore, the linear cross between α and β bands forms the nodal line protected by horizontal mirror symmetry. The detailed scan of band structures also shows that crossing points generated by band crossing are not isolated, but are nodal lines centered at the S point. More band crossing points can be observed throughout the BZ if symmetry effects are considered. Thus, we observed a nodal line throughout the BZ (Fig. 4(e)).

Figure 4(d) shows the band structure with SOC. We found that the linear dispersion of the Dirac cone is barely affected and only the tiny band gaps of 8 meV and 9 meV are opened at R_1 and R_2 points when SOC is turned on. It is worth noting that the topological properties of a system are usually studied because it involves Dirac cones. SOC causes R_1 and R_2 around the S point to open gaps (Fig. 4(d)), and the gaps are only 8 meV and 9 meV, respectively, which is due to the weaker SOC strength of the B atom. To check non-trivial topological characteristics of the ZnB film, we calculated edge states and

the Z_2 invariant of the system (Fig. 5). The half-infinite length Green functions are used to calculate total and spin-polarized edge densities of states by maximally localized Wannier functions (MLWFs). We can see that the gapless edge state connects upper and lower bands of the overall gap (Fig. 5(a)). As shown in Fig. 5(b), two edge states with opposite propagation directions show opposite spin polarizations (red and blue indicate spin up and spin down, respectively) according to the spin momentum lock of the one-dimensional spiral electron. The Z_2 invariant further confirms the topological properties of ZnB. It can be seen from Fig. 5(c) that the number of intersections between any horizontal reference line and WCC evolution line is odd times, so $Z_2 = 1$. These confirm that the ZnB monolayer is a 2D topological insulator.

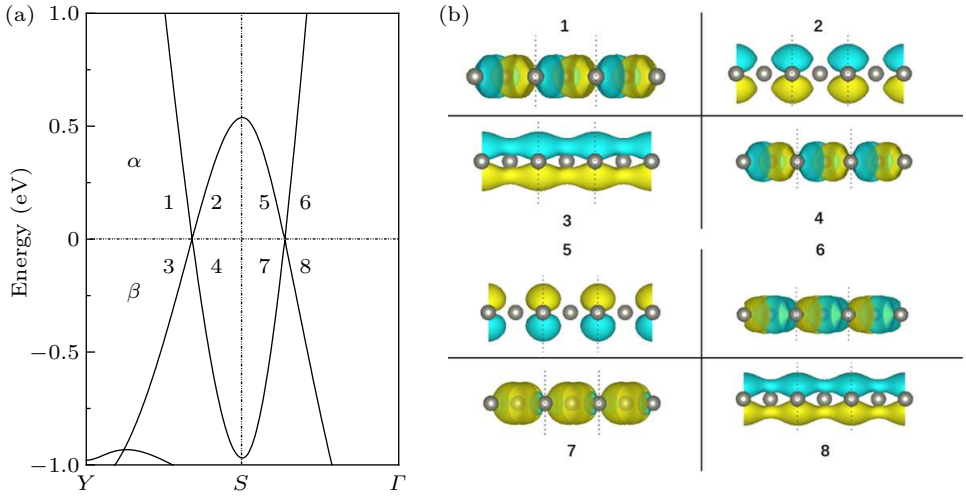


Fig. 3. (a) The calculated band structure of the ZnB monolayer. (b) The real part of Kohn–Sham wave functions near band crossing points.

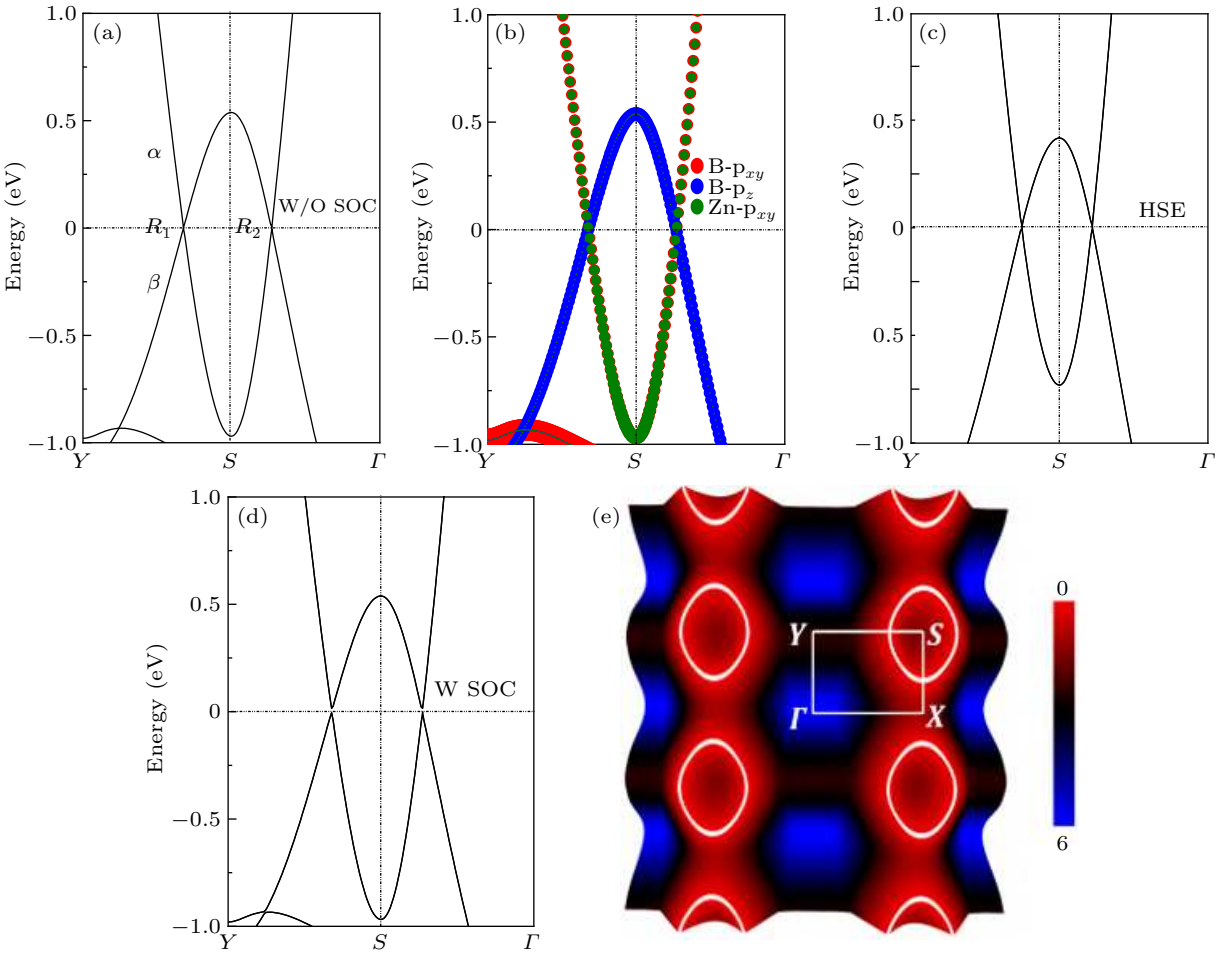


Fig. 4. (a) The calculated band structure for monolayer ZnB without SOC using the DFT + U method. (b) The projection of the bands onto atomic orbitals. (c) Band structure without SOC of ZnB calculated using the HSE06 method. (d) The calculated band structure with SOC. (e) The shapes of the nodal lines obtained by DFT calculation in the Brillouin zone.

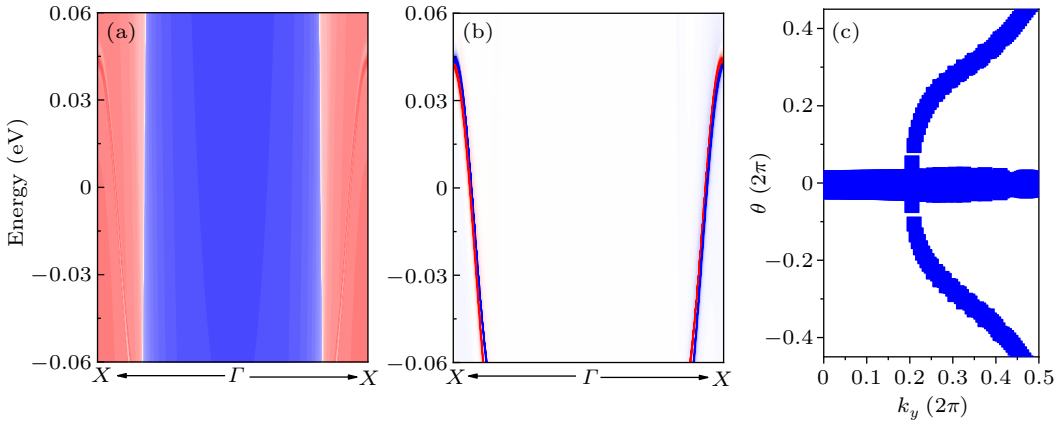


Fig. 5. (a) and (b) The total and spin-polarized edge densities of states for ZnB, respectively. (c) Evolutions of Wannier centers for ZnB along k_y in the spin edge plot. The red and blue lines denote the spin up and down polarization, respectively.

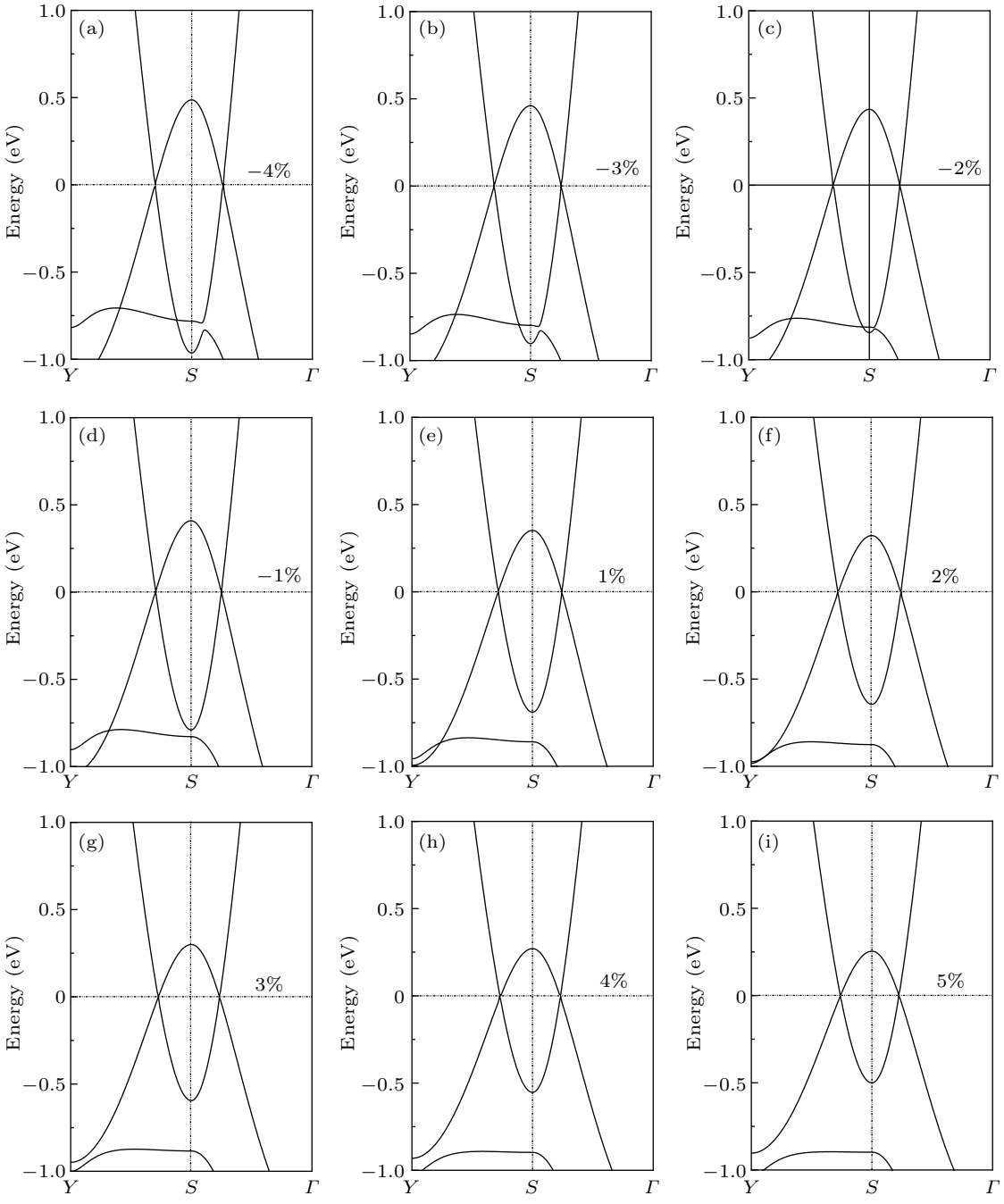


Fig. 6. Band structures of the ZnB monolayer under −4% in-plane compressive strain to 5% tensile strain.

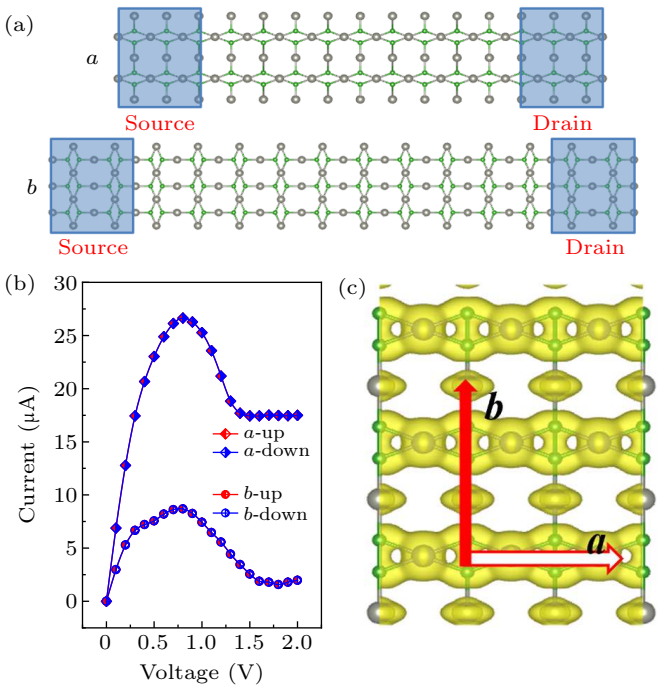


Fig. 7. (a) Schematic illustrations of the ZnB transporting device model along the *a* and *b* directions. (b) The spin-resolved *I*–*V* curves of ZnB along the *a* and *b* directions. (c) Band decomposed charge densities of ±0.5 eV around the Fermi level.

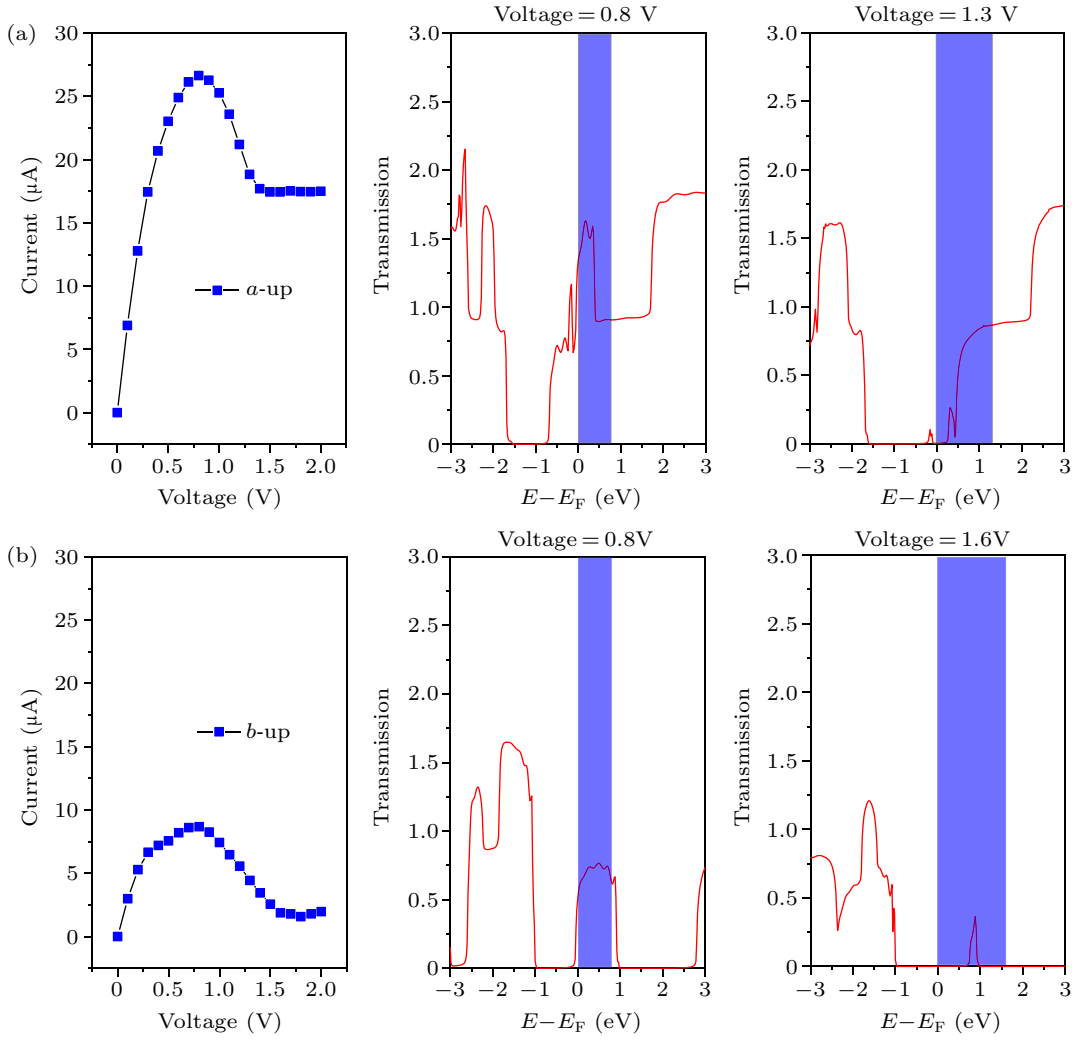


Fig. 8. The calculated transmission spectra of ZnB along the (a) *a* and (b) *b* directions, respectively. The shadowed areas are the bias energy windows in which the states can contribute to transport.

We further examined the robustness of the nodal line under biaxial strain. Up to −4% in-plane compressive strain and 5% tensile strain are applied on the ZnB monolayer, respectively, and the band structures are plotted in Fig. 6. It was found that nodal lines still exist under these strains, indicating that they are robust under mechanical deformation and plane pressure.

There are many ways to calculate transport properties.[51] We use first principle and nonequilibrium Green's function methods to calculate. This method has been used in various articles, such as a Au/GeSi/Au transport junction,[52] zigzag graphene nanoribbon[53] and nanoribbons with adsorbed transition metal atoms,[54] which have been proved to be reliable. Figure 7(a) shows the 2D transporting device models based on the ZnB lattice along the a and b directions. We draw spin-resolved voltage–curve (I–V) curvatures (Fig. 7(b)) by applying a source–drain bias voltage of 0 V to 2.0 V in the a and b directions, respectively. We artificially create a voltage drop by adjusting the chemical potential of the electrodes at both ends. Obviously, the transmission along the a direction is significantly stronger than the b direction in the conductive channel, which can be explained by comparing charge densities at the Fermi level (Fig. 7(c)). The overlaps of wave functions along the a direction are stronger than that along the b direction, resulting in better conductivity in the a direction. It is interesting that the transport characteristics of ZnB are the negative differential resistance (NDR) effect after 0.8 V along the a (b) direction. As can be seen from the transmission spectrum shown in Fig. 8, when the voltage along the a/b direction does not exceed 0.8 V, the current increases with the increase in voltage. When the voltage exceeds 0.8 V, the current decreases rapidly as the voltage increases. This phenomenon is known as the NDR effect

$$I = \frac{2e}{h}\int \mathrm{d}E_{\mathrm{F}} T_{\mathrm{LR}}(E_{\mathrm{F}})[f_{\mathrm{L}}(E_{\mathrm{F}}) - f_{\mathrm{R}}(E_{\mathrm{F}})]. \tag{6}$$

Here, $f_{\mathrm{L(R)}}(E_{\mathrm{F}})$ is the Fermi distribution function of the left and right wires. The transmission coefficient $T_{\mathrm{LR}}(E_{\mathrm{F}})$ can be calculated from $\mathrm{Tr}[\Gamma_{\mathrm{L}} G \Gamma_{\mathrm{R}} G^{+}](E_{\mathrm{F}})$, where $T_{\alpha}(E_{\mathrm{F}}) = \mathrm{i}[\Sigma'_{\alpha}(E_{\mathrm{F}}) - \Sigma^{\mathrm{a}}_{\alpha}(E_{\mathrm{F}})]$ is the line width function, and $\Sigma^{\mathrm{a}}_{\alpha}(E_{\mathrm{F}})$ represents the self-energy.

According to the above Landauer–Biittiker formula, the large difference between the current and voltage curves of the device is analyzed. The current is the integral area of the electron transmission curve within the bias window. When the integral area of the transmission curve of electrons passing through the local window becomes smaller, the current drops. As the voltage increases, the current decreases, resulting in the negative differential resistance effect. An interesting transfer characteristic of ZnB is the NDR at the voltage of 0.8 V. According to the analysis on the transmission spectrum shown in Fig. 8, the NDR effect can be explained by comparison between the increase in the energy window and the decrease in transmission from 0.8 V to 1.3 V (1.6 V) along the a (b) direction. It can be seen that energy windows become wider and the transmission decreases as the bias voltage increases from 0.8 V to 1.3 V (1.6 V) along the a (b) direction; therefore, the NDR effect is generated.

This effect is a fundamental characteristic of electronic devices such as esala tunneling diodes, which have wide applications in oscillator fast switching and frequency-locked circuits.

4. Conclusion and perspectives

We confirmed that 2D tetragonal ZnB is a nodal-line semimetal with great transport properties. Two bands, mainly composed of p_{xy} orbitals of Zn and B atoms and the p_z orbitals of the B atom, cross at the Fermi surface. This causes ZnB to present a nodal line centered on the S point in its BZ. And the band structure is protected by the mirror inversion symmetry and p_{xy}/p_z band cross. We further examined the robustness of the nodal line under biaxial strain by applying up to −4% in-plane compressive strain and 5% tensile strain on the ZnB monolayer, respectively. We also found an interesting NDR effect when studying its transport properties. Our research has opened a path for the study of Dirac physics and spintronics and the fabrication of new quantum devices.

Acknowledgments

Project supported by the Natural Science Foundation of Shandong Province, China (Grant No. ZR2019MA041), Taishan Scholar Project of Shandong Province, China (Grant No. ts20190939), and the National Natural Science Foundation of China (Grant No. 62071200).

References

[1] Yazyev O V 2013 *Acc. Chem. Res.* **46** 2319
[2] Butler S Z, Hollen S M and Cao L 2013 *ACS Nano* **7** 2898
[3] Bhimanapati G R, Lin Z, Meunier V, Jung Y, *et al.* 2015 *ACS Nano* **9** 11509
[4] Novoselov K S, Mishchenko A, Carvalho A and Castro Neto A H 2016 *Science* **353**
[5] Kassem A T 2013 *IOSR J. Appl. Chem.* **6** 45
[6] Castro Neto A H, Guinea F, Peres N M R, Novoselov K S and Geim A K 2009 *Rev. Mod. Phys.* **81** 109
[7] Titheridge J E 1998 *J. Geophys. Res. Space Phys.* **103** 2261
[8] Bliokh Y P, Freilikher V and Nori F 2013 *Phys. Rev. B* **87** 245134
[9] Wang L, Meric I, Huang P Y, Gao Q, Gao Y, Tran H, Taniguchi T, Watanabe K, Campos L M, Muller D A, Guo J, Kim P, Hone J, Shepard K L and Dean C R 2013 *Science* **342** 614
[10] Yu R, Zhang W, Zhang H J, Zhang S C, Dai X and Fang Z 2010 *Science* **329** 61
[11] Zhang C W and Yan S S 2012 *J. Phys. Chem. C* **116** 4163
[12] Wang Z, Zhou X F, Zhang X, Zhu Q, Dong H, Zhao M and Oganov A R 2015 *Nano Lett.* **15** 6182
[13] Li S S, Ji W X, Hu S J, Zhang C W and Yan S S 2017 *ACS Appl. Mater. Interfaces* **9** 41443

[14] Zhang W, Wu Q, Yazyev O V, Weng H, Guo Z, Cheng W D and Chai G L 2018 *Phys. Rev. B* **98** 1
[15] Yuan D, Hu Y, Yang Y and Zhang W 2021 *Chin. Phys. Lett.* **38** 117301
[16] Li W, Zhang G and Guo M 2014 *Nano Research* **7** 518
[17] Zhang L, Zhang S F, Ji W X, Zhang C W, Li P, Wang P J, Li S S and Yan S S 2018 *Nanoscale* **10** 20748
[18] Wu Y, Wang L L, Mun E, Johnson D D, Mou D, Huang L, Lee Y, Bud'ko S L, Canfield P C and Kaminski A 2016 *Nat. Phys.* **12** 667
[19] Schoop L M, Ali M N, Straßer C, Topp A, Varykhalov A, Marchenko D, Duppel V, Parkin S S P, Lotsch B V and Ast C R 2016 *Nat. Commun.* **7** 11696
[20] Weng H, Liang Y, Xu Q, Yu R, Fang Z, Dai X and Kawazoe Y 2015 *Phys. Rev. B* **92** 045108
[21] Yu R, Weng H and Fang Z 2015 *Phys. Rev. Lett.* **115** 036807
[22] Jin Y J, Wang R, Zhao J Z, Du Y P, Zheng C Di, Gan L Y, Liu J F, Xu H and Tong S Y 2017 *Nanoscale* **9** 13112
[23] Wirth G, ÖlschlÏger M and Hemmerich A 2011 *Nat. Phys.* **7** 147
[24] Li S, Liu Y, Wang S S, Yu Z M, Guan S, Sheng X L, Yao Y and Yang S A 2018 *Phys. Rev. B* **97** 1
[25] Zhou P, Ma Z S and Sun L Z 2018 *J. Mater. Chem. C* **6** 1206
[26] Zhong C, Wu W, He J, Ding G, Liu Y, Li D, Yang S A and Zhang G 2019 *Nanoscale* **11** 2468
[27] Feng B, Fu B, Kasamatsu S, *et al.* 2017 *Nat. Commun.* **8** 8
[28] Pang Z X, Zhao Y C, Ji W X, Wang Y and Li P 2021 *Phys. Chem. Chem. Phys.* **23** 12280
[29] Mounet N, Gibertini M, Schwaller P, Campi D, Merkys A, Marrazzo A, Sohier T, Castelli I E, Cepellotti A, Pizzi G and Marzari N 2018 *Nat. Nanotechnol.* **13** 246
[30] Hu Y, Li S S, Ji W X, Zhang C W, Ding M, Wang P J and Yan S S 2020 *J. Phys. Chem. Lett.* **11** 485
[31] Schmidt P, Haas S and Levi A F J 2006 *Appl. Phys. Lett.* **88** 013502
[32] Tsu R and Esaki L 1973 *Appl. Phys. Lett.* **22** 562
[33] Ismail M and Kim S 2020 *Appl. Surf. Sci.* **530** 147284
[34] Kresse G and Furthmüller J 1996 *Comput. Mater. Sci.* **6** 15
[35] Kresse G and Hafner J 1993 *Phys. Rev. B* **47** 558
[36] Langreth D C and Mehl M J 1983 *Phys. Rev. B* **28** 1809
[37] Perdew J P, Burke K and Ernzerhof M 1996 *Phys. Rev. Lett.* **77** 3865
[38] Joubert D 1999 *Phys. Rev. B* **59** 1758
[39] Becke A 1988 *Phys. Rev. A* **38** 3098
[40] Heyd J, Scuseria G E and Ernzerhof M 2003 *J. Chem. Phys.* **118** 8207
[41] Togo A, Oba F and Tanaka I 2008 *Phys. Rev. B* **78** 134106
[42] Dudarev S and Botton G 1998 *Phys. Rev. B* **57** 1505
[43] Baker J M 1971 *J. Phys. C Solid State Phys.* **4** 930
[44] Ozaki T, Nishio K and Kino H 2010 *Phys. Rev. B* **81** 035116
[45] Ozaki T 2007 *Phys. Rev. B* **75** 035123
[46] Kulish V V and Huang W 2017 *J. Mater. Chem. C* **5** 8734
[47] Andrew R C, Mapasha R E and Ukpong A M 2012 *Phys. Rev. B* **85** 125428
[48] Peng R, Ma Y, Huang B and Dai Y 2019 *J. Mater. Chem. A* **7** 603
[49] Mouhat F and Coudert F X 2014 *Phys. Rev. B* **90** 224104
[50] Zhang X, Wang A and Zhao M 2015 *Carbon N. Y.* **84** 1
[51] Landauer R 1981 *Phys. Lett. A* **85** 91
[52] Liu N, Zhang L, Chen X, Kong X, Zheng X and Guo H 2016 *Nanoscale* **8** 16026
[53] Zhang L, Zhao J, Cheng N and Chen Z 2020 *Phys. Chem. Chem. Phys.* **22** 3584
[54] Fu X X, Niu Y, Hao Z W, Dong M M and Wang C K 2020 *Phys. Chem. Chem. Phys.* **22** 16063